The Astrophysical Journal, 900:74 (16pp), 2020 September 1 https://doi.org/10.3847/1538-4357/aba94c

Kinetic Simulations of the Jovian Energetic Ion Circulation around Ganymede

Christina Plainaki[1], Stefano Massetti[2], Xianzhe Jia[3], Alessandro Mura[2], Anna Milillo[2], Davide Grassi[2], Giuseppe Sindoni[1], Emiliano D'Aversa[2], and Gianrico Filacchione[2]
[1] Agenzia Spaziale Italiana—ASI, Via del Politecnico, I-00133, Rome, Italy; christina.plainaki@asi.it
[2] INAF-IAPS, Via del Fosso del Cavaliere 100, I-00133, Rome, Italy
[3] Department of Climate and Space Sciences and Engineering, University of Michigan, Ann Arbor, MI 48109-2143, USA
Received 2020 May 2; revised 2020 July 24; accepted 2020 July 25; published 2020 September 2

Abstract

The temporal and spatial variability of the radiation environment around Ganymede has a direct impact on the moon's exosphere, which links Jupiter's magnetosphere with the satellite's icy surface. The dynamics of the entry and circulation inside Ganymede's magnetosphere of the Jovian energetic ions, as well as the morphology of their precipitation on the moon's surface, determine the variability of the sputtered-water release. For this reason, the so-called planetary space weather conditions around Ganymede can also have a long-term impact on the weathering history of the moon's surface. In this work, we simulate the Jovian energetic ion precipitation to Ganymede's surface for different relative configurations between the moon's magnetic field and Jupiter's plasma sheet using a single-particle Monte Carlo model driven by the electromagnetic fields from a global MHD model. In particular, we study three science cases characterized by conditions similar to those encountered during the NASA Galileo G2, G8, and G28 flybys of Ganymede (i.e., when the moon was above, inside, and below the center of Jupiter's plasma sheet). We discuss the differences between the various surface precipitation patterns and the implications in the water sputtering rate. The results of this preliminary analysis are relevant to ESA's JUICE mission and in particular to the planning and optimization of future observation strategies for studying Ganymede's environment.

Unified Astronomy Thesaurus concepts: Galilean satellites (627); Planetary magnetosphere (997); Jovian satellites (872); Space weather (2037); Solar system (1528)

1. Introduction and Motivation for the Current Work

Jupiter's moon Ganymede is the only natural satellite in the solar system with an intrinsic dipole magnetic field (Gurnett et al. 1996; Kivelson et al. 1996, 1997). At Ganymede's orbital distance (~15 R_J, with R_J being Jupiter's radius), the Jovian magnetospheric plasma confined by the planet's magnetic field approximately corotates with Jupiter at a velocity of ~ 150 km s^{-1} (Williams 2001; Kivelson et al. 2004; Bagenal et al. 2016), overtaking the moon, which moves with an orbital velocity of ~11 km s^{-1} (both velocities have counterclockwise direction, as seen from the North). The magnetic field of Ganymede partially shields the surface from ion impacts, especially at equatorial latitudes (e.g., Kivelson et al. 1997). The dynamics of plasma entry and circulation inside Ganymede's magnetosphere, as well as the properties of the ion precipitation to the surface, are primarily controlled by the reconnection between Jupiter's and Ganymede's magnetic fields (Jia et al. 2010b). With the magnetic axis tilted by ~10° with respect to its rotational axis, Jupiter's plasma sheet (JPS), which is confined by the magnetic field, oscillates up and down at the satellite's orbit (Kivelson et al. 1998; McGrath et al. 2013), resulting in a dynamic configuration of the circulation and surface precipitation patterns of the different ion populations. The energetic component of the Jovian magnetospheric population is characterized by H^+, O^{n+}, and S^{n+} ions (Paranicas et al. 1999; Cooper et al. 2001; Mauk et al. 2004), as evidenced by the NASA Galileo Energetic Particle Detector (EPD) observations, which detected ions in the 20 keV–55 MeV energy range (Williams et al. 1992; Paranicas et al. 1999; Mauk et al. 2004).

Past work on modeling Ganymede's ion environment has revealed that the bulk population of Jupiter's plasma enters the moon's magnetosphere mainly through the cusps and at low latitudes in the plasma wake hemisphere (that is, the leading hemisphere), most likely through tail magnetic reconnection (e.g., Williams et al. 1997; Poppe et al. 2018). The maximum ion precipitation to the surface is expected to take place near the open–closed magnetic field line boundary (OCFB) regions (e.g., Kivelson et al. 1997; Plainaki et al. 2015; Fatemi et al. 2016). Energetic ion fluxes (mainly hydrogen and multiply charged oxygen and sulfur ions) can actually activate complex processes, such as sputtering and radiolysis, releasing H_2O, O_2, H_2, as well as H, O, and OH particles (Johnson 1990; Marconi 2007; Plainaki et al. 2015; Leblanc et al. 2017). At Ganymede, and also at Europa, direct sputtering of surface water molecules, together with water sublimation and radiolysis (leading mainly to O_2 and H_2 release), generate a tenuous atmospheric envelope around the moon, often referred to as an "exosphere" (e.g., Plainaki et al. 2015, 2018). Observations by the Plasma Science (PLS; Frank et al. 1997; Collinson et al. 2018) and Plasma Wave Science (PWS; Eviatar et al. 2001) instruments on board the Galileo spacecraft also revealed the existence of an ionosphere at Ganymede (Carnielli et al. 2019), consistent with the findings of the Galileo radio occultation experiment (Kliore 1998). Figure 1 shows the possible source and loss mechanisms for the exosphere of Ganymede, coupling the moon's space environment with the Jovian magnetosphere.

Recent efforts based both on data of past missions (e.g., NASA Galileo) and modeling techniques have been focused on the study of ion precipitation to Ganymede's surface. Plainaki et al. (2015) performed single-particle Monte Carlo (MC) simulations of the circulation and precipitation to Ganymede's surface of Jovian energetic ions using electric and magnetic fields from the magnetohydrodynamic (MHD) models of Jia et al. (2008, 2009). The results presented by these authors

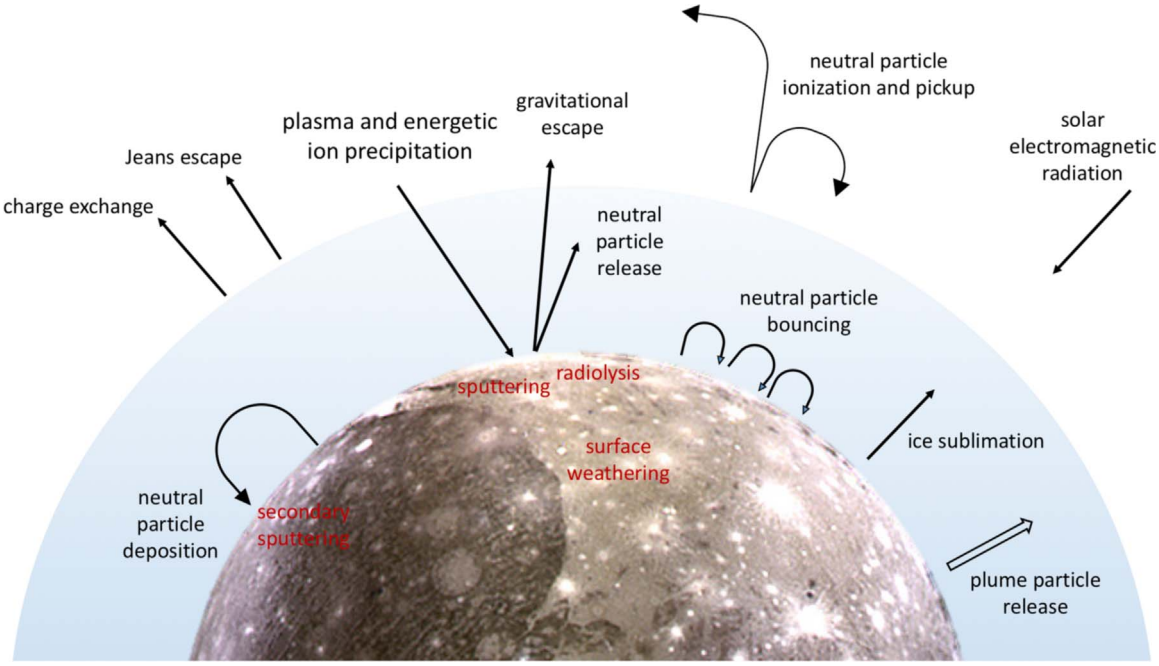

Figure 1. Possible source and loss mechanisms for the exosphere of Ganymede. The moon's environment is strongly coupled with the Jovian magnetosphere through a series of dynamical processes that contribute to the overall energy exchange between the two systems. Ganymede image credit: NASA/JPL/DLR.

corresponded to magnetic and electric field conditions similar to those during the G8 flyby of Galileo and referred only to singly charged oxygen, sulfur, and hydrogen ions in the energy range from 1 to 100 keV. The generated ion precipitation maps showed the existence of a shielded region close to the trailing-hemisphere surface (at distances smaller than $\sim$1.5 R_G from the moon's center) and enhancements in the ion flux at near-surface altitudes above the low-latitude leading hemisphere (Plainaki et al. 2015, 2020), a result that was further confirmed by other studies as well (e.g., Fatemi et al. 2016; Poppe et al. 2018; Carnielli et al. 2020). The trajectories of the higher-energy ions were shown to be less affected by Ganymede's magnetic field. We note that in the numerical simulations by Plainaki et al. (2015), a "full ion mirroring" condition was included in the code, allowing the ions to be reflected back from both the top and bottom sides of the simulation box.

The three-dimensional self-consistent hybrid model by Fatemi et al. (2016) examined the kinetic effects of the Jovian plasma interaction with Ganymede's magnetosphere. The model succeeded in capturing both Hall-related and finite Larmor radius effects in the ion circulation within Ganymede's magnetosphere through the inclusion of the Hall term, although a higher spatial resolution would allow more detailed features to be revealed (Dorelli et al. 2015; Tóth et al. 2016; Zhou et al. 2019). The simulations by Fatemi et al. (2016) were based on parameter values given by Jia et al. (2008). The model results reproduced well the Galileo magnetometer measurements taken during each of the six Galileo flybys. Fatemi et al. (2016) also estimated the precipitating flux of H^+, O^{++}, and S^{+++} ions with energies between 1 and 10^4 keV, applying a forward-tracing technique using the modeled field values. Their results showed that ions precipitate predominantly at the moon's polar cap region along open field lines. Moreover, the ion precipitation maps in Fatemi et al. (2016) were in good agreement with Ganymede's surface brightness map by Khurana et al. (2007). We note that the results on ion precipitation presented by Fatemi et al. (2016) corresponded to conditions similar to those during the G8 flyby. The work on the ion precipitation maps by Fatemi et al. (2016) was further extended by Poppe et al. (2018), who used the combination of electric and magnetic fields derived from the hybrid simulations of Ganymede's magnetosphere by Fatemi et al. (2016) and a backwards Liouville tracing technique (e.g., Cooper et al. 2001; Allioux et al. 2013) to quantify the dynamics of thermal and energetic ions near Ganymede. The model of these authors confirmed previous results on the existence of a shielded equatorial region on Ganymede's trailing hemisphere and a nonnegligible ion precipitation in the low-latitude leading hemisphere. The simulation method used in the work by Poppe et al. (2018) was focused on field conditions at Ganymede representative of the Galileo G8 flyby. Leblanc et al. (2017) studied the generation mechanisms and evolution of Ganymede's neutral environment also taking into account the gravitational influence by Jupiter. Their MC model followed the dynamical evolution of the exosphere as Ganymede orbits Jupiter, assuming that Jovian ions precipitate to the surface within the open field line regions and considering the OCFB as derived by the auroral observations described in McGrath et al. (2013). Although in the model by Leblanc et al. sputtering and radiolysis were considered among the source mechanisms for the exosphere generation, no variation of the precipitating flux with respect to JPS was considered.

In this paper, for the first time, we perform energetic ion trajectory computations for three distinct configurations between Ganymede's magnetic field and JPS, characterized by magnetic and electric field conditions similar to those during the G2, G8, and G28 flybys of Galileo (i.e., the moon above, inside, and below the center of JPS). For each of the aforementioned configurations, we estimate the ion precipitation to the surface for different ion species (H^+, O^{++}, and S^{+++}) in a total energy range from 1 keV to 3 MeV, assuming the energy spectra retrieved by Paranicas et al. (1999). We note that simulating the circulation of the highly charged component of Jupiter's magnetosphere near Ganymede is very important

since the energetic ionic environment is dominated mainly by a combination of H^+, O^{++}, and S^{+++} (Collier & Hamilton 1995; Keppler & Krupp 1996; Mauk et al. 2004). The thermal ion population provides no significant contribution to the flux precipitating in the upstream hemisphere of Ganymede (Poppe et al. 2018), whereas the energetic ion flux precipitating to the moon controls surface weathering (e.g., Johnson 1990; Shi et al. 1995; Hansen & McCord 2004; Khurana et al. 2007), as well as the production of radiolytic species in the upper surface layers (e.g., Cooper et al. 2001; Gomis et al. 2004; Teolis et al. 2017) and sputtering (e.g., Hall et al. 1998; Marconi 2007; Turc et al. 2014; Plainaki et al. 2015). Moreover, to assess the energy exchange between the Jovian magnetosphere and Ganymede, estimating the energetic ion precipitation rate over the entire surface is necessary. To this end, and also to globally understand the properties of the exospheric environment, we need to get an in-depth view of the role of the energetic ion environment in provoking the direct release of surface particles or/and in activating chemical reactions that lead to particle emissions. The short- or long-term interaction of Jovian ions with the icy surface not only depends on the characteristics of the surface itself (composition, ice state, temperature) but also on the exact way—in terms of impinging flux spatial distribution—the moon gets bombarded by the JPS environment (planetary space weather; Plainaki et al. 2016, 2018, 2020). In this view, in the current paper, we focus on the study of the surface precipitation of the Jovian energetic ion population. The paper is organized as follows. In Section 2, we describe the model of ion circulation within Ganymede's magnetosphere. The results of the simulations are presented in Section 3, whereas in Section 4 we analyze the differences between the various ion precipitation patterns corresponding to different configurations of Ganymede's field with respect to JPS, and we discuss the implications in Ganymede's exosphere generation and surface-weathering history from a planetary space weather perspective.

2. Model Description

To obtain the spatial distribution of the energetic ion circulation around Ganymede and to map their precipitation to the surface, we apply a single-particle MC model based on the technique previously proposed by Plainaki et al. (2015) assuming a background magnetic field configuration. In particular, we use the magnetic and electric field data derived from the Jia et al. (2008, 2009) global MHD model of Ganymede's magnetosphere, which has been shown to reproduce with high fidelity the magnetic field and plasma measurements during multiple Galileo flybys of Ganymede. We assume that the energetic component of the Jovian magnetospheric population is characterized by H^+, O^{n+}, and S^{n+} ions (Cooper et al. 2001; Mauk et al. 2004).

We trace the trajectories of Jovian ions of different species for the full three-dimensional ion velocity distribution. In addition to the simulations performed in Plainaki et al. (2015), in the current paper we calculate the trajectories of multiply charged ions (e.g., O^{++}, S^{+++}) at discrete energies covering the range from 1 to 3000 keV. In our simulations, the standard "GphiO" coordinate system is used: X is along Ganymede's orbital motion (and the JPS flow direction, too), Z is along Jupiter's spin axis, and Y points toward Jupiter. The $\pm 10 \times \pm 10 \times \pm 10$ R_G simulation box is centered on the moon (with $R_G = 2634$ km being Ganymede's radius), with a spatial resolution of 0.1 R_G, for a total of 8×10^6 cells. In each run, 2×10^6 test particles are launched with a defined initial energy but random initial directions: to simulate the ions populating JPS, which corotates with Jupiter faster than Ganymede along its orbit and then overtakes and embeds the moon, we place a 1 R_G thick planar "source surface" perpendicular to the moon's orbit, located between $X = -3$ R_G and $X = -4$ R_G upstream of Ganymede (the standoff distance of the magnetopause is ~ 2 R_G). Particle tracking is achieved via the Boris–Buneman Lorentz force integrator (Boris 1970) over the gridded magnetic and electric field data output from the published MHD simulations, which is interpolated within each cell. Weighted physical quantities associated with each moving test particle are stored into a $200 \times 200 \times 200 \times 6$ array, resulting in a 3D distribution of density, energy, and velocity Cartesian components, and $\boldsymbol{V}$ parallel to the $\boldsymbol{B}$ component. Test particles ending their paths by hitting the body surface populate a 180×360 array, resulting in a latitude per longitude distribution of ion impacts, energy, and flux. JPS ions do not simply corotate; they also bounce back and forth along the magnetic field lines of Jupiter: to model this motion within our simulation box, we enforce all the ions exiting through the top and bottom sides of the box ($Z = \pm 10 R_G$), along the magnetic field lines, to be reflected back (full mirroring), because we expect that they actually do that once they reach their mirror point (which is located outside the box). In the code, this is achieved by changing sign at the z component of the test particle speed (as in Plainaki et al. 2015). It must be noted that allowing the ions to freely escape the simulation box along the open magnetic field line (connected to Jupiter) would lead to an underestimation of the ion circulation and ion precipitation into the polar caps, which would not be compatible with current knowledge. Because Ganymede is embedded within JPS, about $3R_J \cong 80R_G$ thick at its orbit (Kivelson et al. 2004), ions are expected to (re)enter the simulation box, bouncing back somewhere along the field lines connected to Jupiter, or spreading in from the contiguous region of JPS. Because of our "full mirroring" assumption, the results in this work have to be considered as upper limits for the ion circulation around Ganymede and interpreted consequently, as a fraction of the ions bouncing along the field lines can actually get lost and may not re-enter back into the simulation box.

In this paper, for the first time, we perform ion trajectory computations for three sets of MHD simulation data corresponding to three different configurations of Ganymede's magnetic field with respect to JPS, characterized by magnetic and electric field conditions similar to those during the G2 (science case (i)), G8 (science case (ii)), and G28 (science case (iii)) flybys of Galileo. The trajectories during the Galileo G2, G8, and G28 flybys of Ganymede are discussed in Jia et al. (2010a). We define, accordingly, the following science cases:

1. science case (i): Ganymede is above the center of JPS
2. science case (ii): Ganymede is close to the center of JPS
3. science case (iii): Ganymede is below the center of JPS.

For each one of the aforementioned science cases, we run simulations for H^+, O^{++}, and S^{+++} at the discrete energies of 1, 5, 10, 30, 50, 100, 300, and 3000 keV. To normalize the simulation results and get the absolute flux of ions precipitating to the surface (in $cm^{-2}\,s^{-1}\,keV^{-1}$), we insert in our code the species-specific distributions as determined by Paranicas et al. (1999). We note that the spectra by Paranicas et al. (1999) were

obtained based on data from both the Galileo EPD and PLS instruments, which together cover a range from 1 eV to tens of MeV with some overlap of coverage in the tens of the keV range. Paranicas et al. (1999) also showed that their fits of the energetic ion spectra were compatible with the PLS data in the energy range from 1 keV to tens of keV. Although the existence of a thermal component in the lower-energy range cannot be excluded, we consider that the spectra by Paranicas et al. covering the 1 keV–3 MeV range are representative of the energetic ion population at Ganymede. We considered an additional 1:5 scaling of the fluxes above and below the center of JPS (science cases (i) and (iii), respectively), with respect to the ones near the center of JPS (science case (ii)), to take into account the relative densities at the orbit of Ganymede, as reported in Kivelson et al. (2004).

3. Results

Figure 2 presents snapshots in the *XY, XZ*, and *YZ* planes of the H^+ flux at initial energy equal to 10 keV for the three considered science cases. The ion circulation and surface precipitation patterns in Figure 2 are compatible with a flow mainly through the cusps and the polar caps, guided strongly by the position of the OCFB. A relatively smaller contribution in the low-latitude surface precipitation at the leading side comes from the ions drifting around the moon, populating the magnetotail. The surface precipitation of H^+ is in general asymmetric with respect to the leading and trailing hemispheres, as well as the Jupiter- and anti-Jupiter-facing sides of Ganymede's surface. In all three science cases, the surface precipitation of H^+ takes place at higher latitudes at the trailing side with respect to the leading one (see panels (b), (e), and (h) in Figure 2).

The presence of Alfvén wings that bend the open magnetic field lines above Ganymede's polar caps is evident in Figure 2. Their form is different for the three considered science cases. Comparing science cases (i) and (iii), we note that the form and the position of the Alfvén wings are not perfectly anti-asymmetric (see also Jia et al. 2008). In particular, as shown in panels (b) and (h), the Alfvén wings are significantly wider and more elongated in science case (iii). In general, the H^+ flux decreases considerably inside Ganymede's magnetosphere, especially in the upstream region shielded by the closed magnetic field lines (see, for instance, Figure 2, panels (b), (e), and (h)). However, the flux inside the Alfvén wings appears increased compared to the one above the low-latitude upstream hemisphere; regions of lower ion intensity, nevertheless, also appear there (see panels (c) and (i) in Figure 2). In science case (ii), the relative increase of the H^+ flux inside the Alfvén wings is higher with respect to the other two cases, a fact that reflects the higher ion densities near the center of JPS (Kivelson et al. 2004).

As shown in panels (a) and (g) of Figure 2 (*XY* plane snapshots corresponding to science cases (i) and (iii), respectively) and also in panels (c) and (i) (*YZ* plane snapshots corresponding to science cases (i) and (iii), respectively), there is a significant asymmetry between the Jupiter- and the anti-Jupiter-facing sides in the H^+ precipitation to high-latitude and polar cap surface regions. Such an asymmetry is in the opposite sense for science cases (i) and (iii) and for the northern and southern hemispheres. In particular, in science case (i), the high-latitude/polar cap surface of the anti-Jupiter-facing side of the northern hemisphere receives slightly more intense H^+ fluxes than the opposite side (see panels (a) and (c) in Figure 2). In science case (iii), instead, an extended region of the high-latitude and polar cap surface of the Jupiter-facing side of the northern hemisphere is bombarded by more intense H^+ fluxes with respect to the opposite side, which is, to a large extent, shielded from magnetospheric particles (see panels (g) and (i) in Figure 2). The reverse situation takes place at the southern hemisphere; in particular, in science case (i), higher fluxes precipitate at the high-latitude and polar cap surface of the Jupiter-facing side of the southern hemisphere (see panel (c) in Figure 2), whereas in science case (iii), higher fluxes precipitate at the high-latitude and polar cap surface of the anti-Jupiter-facing side of the southern hemisphere (see panel (i) in Figure 2). In science case (ii) (Ganymede is near the center of JPS), the asymmetries in the high-latitude and polar cap surface precipitation are less.

Figure 3 shows the expected H^+ precipitation maps in science case (ii) (Ganymede is near the center of JPS) for different initial ion energies. The W longitude system has been used, meaning the leading hemisphere is at long $\sim 90^0$ and long $\sim 0^0$ is at the Jupiter-facing hemisphere apex. For both north and south hemispheres, there is a trailing–leading asymmetry in the H^+ surface precipitation that gets less marked as the initial ion energy increases (for instance, compare panels (a) and (c) with (d) and (f)).

As seen in both Figures 2 and 3 (which refers to science case (ii)), the H^+ flux diverted around the magnetopause precipitates onto the low-latitude surface of Ganymede delimited by the position of the OCFB. The low-latitude and equatorial H^+ circulations (see panels (c), (f), and (i) of Figure 2), for all the considered science cases, show a more intense flux in the anti-Jupiter direction (negative *Y*-axis in Figure 2). This asymmetry is more apparent in science case (ii), especially in the northern hemisphere. Indeed, Figure 3 shows that the low-latitude and equatorial H^+ flux at the anti-Jupiter-facing side of the northern hemisphere (around longitude $\sim 180°$) reaches lower latitudes than those at the opposite side (around longitude $\sim 0°$), at least for energies up to 100 keV. Also at the southern hemisphere, the fluxes precipitating on the Jupiter- and anti-Jupiter-facing hemispheres are asymmetric. This asymmetry is most evident in the low-latitude and equatorial H^+ fluxes with initial energy up to at least 10 keV.

Figure 4 provides *XZ* projections of the O^+ and O^{++} circulation around Ganymede at initial energy equal to 30 keV for the three considered science cases. The presence of oxygen ions inside the Alfvén wings is caused by two effects: their relatively large rigidity (which is enough to allow ions to partially penetrate), and, at larger extent, the ions bouncing back toward Ganymede, which end up populating the wings due to $E \times B$ drift.

The results presented in Figure 4 confirm that the properties of the surface precipitation of 0xygen ions depend strongly on their actual charge state. Indeed, lower-rigidity O^{++} ions (the magnetic rigidity of an ion is defined as the ratio of its momentum to its charge, i.e., $=mv/q$, where m is the ion mass, v its velocity, and q its charge) are more strongly guided by the magnetic field than O^+, and they reach the low-latitude leading hemisphere with higher fluxes, for all three science cases (see panels (d), (e), and (f) in Figure 4). Equivalently, the surface of the moon's trailing hemisphere (plasma upstream) appears slightly more shielded from O^{++} than from O^+. This applies for our single-particle MC model but in the case of ideal MHD

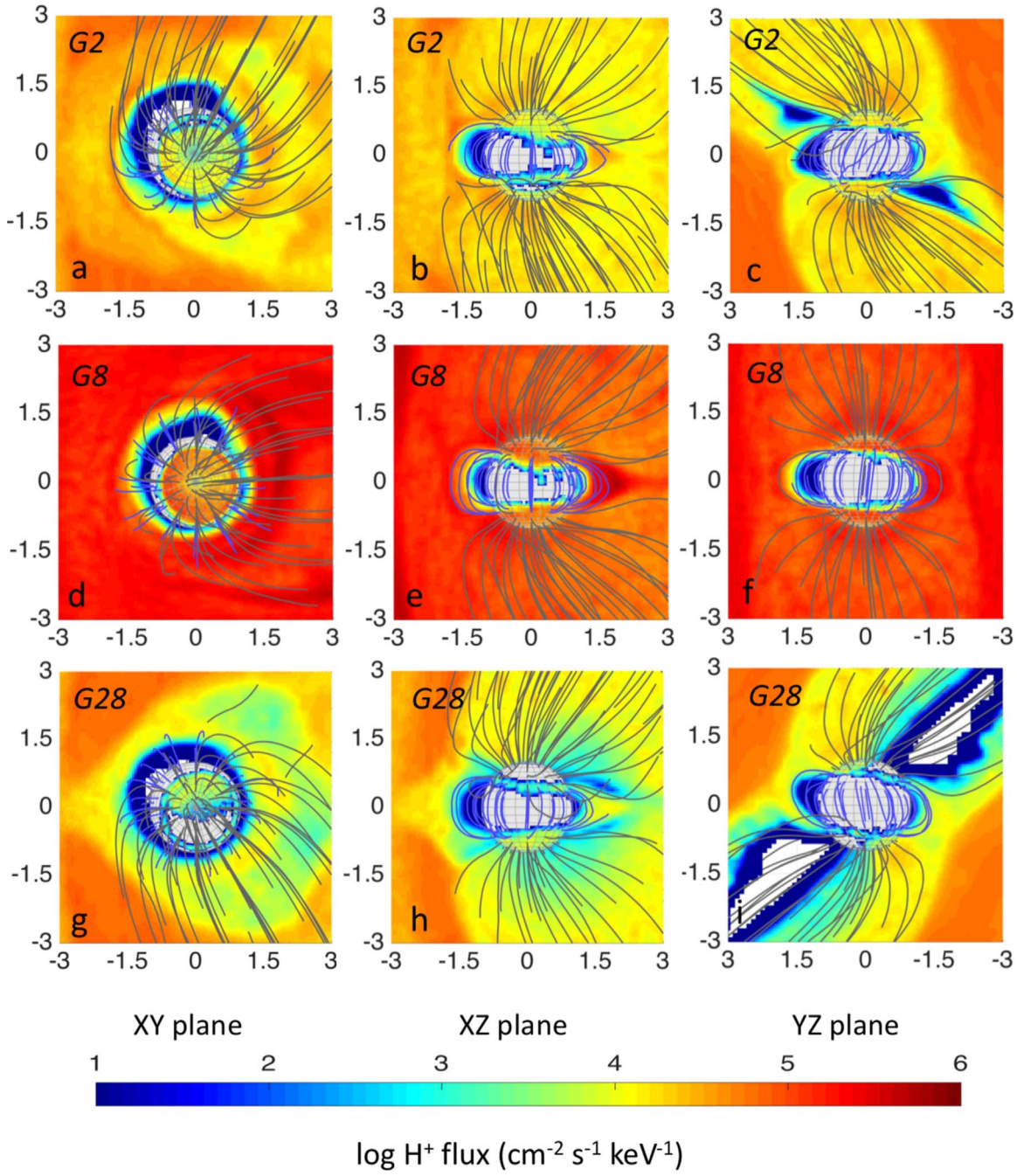

Figure 2. H^+ flux circulation around Ganymede at initial energy equal to 10 keV for three different configurations of the moon's magnetic field with respect to JPS: panels (a), (b), and (c) correspond to science case (i) (Ganymede is above the center of JPS); panels (d), (e), and (f) correspond to science case (ii) (Ganymede is near the center of JPS); panels (g), (h), and (i) correspond to science case (iii) (Ganymede is below the center of JPS). The GPhiO coordinates have been used: *X* is along the ambient flow direction (and Ganymede's orbital motion), *Z* is along the Jupiter's spin axis, and *Y* points toward Jupiter (in units of Ganymede's radii). The first column (panels (a), (d), and (g)) shows the *XY* projections, the second column (panels (b), (e), and (h)) shows the *XZ* projections, and the third column (panels (c), (f), and (i)) shows the *YZ* projections. The two elongated empty areas in panel (i) are shielded regions, where 10 keV H^+ ions cannot enter.

models where ion gyromotion is averaged out and the ions and electrons are combined into a single fluid, such asymmetries would not be present (see also discussion in Paty et al. 2008).

The precipitation patterns in Figure 4 are compatible with a flow through the cusps and polar caps and a mounting number of ions in the downstream region. Indeed, as seen in all three panels of Figure 4, the oxygen ion flow gains access to the surface through the cusps and polar caps and at low latitudes of the wake hemisphere, a result that confirms previous simulations by Paty & Winglee (2004), Paty et al. (2008), Plainaki et al. (2015), and Poppe et al. (2018). In the context of comparative planetary space weather science (see, for instance, discussions in Plainaki et al. 2016 and André et al. 2018), this situation reminds the motion of the ions in the Earth's plasma sheet, in the magnetotail reconnection region (e.g., Chen & Palmadesso 1986). Our simulations show that ions circulating inside Ganymede's magnetosphere can gain access along the closed field lines back to Ganymede's surface in the leading

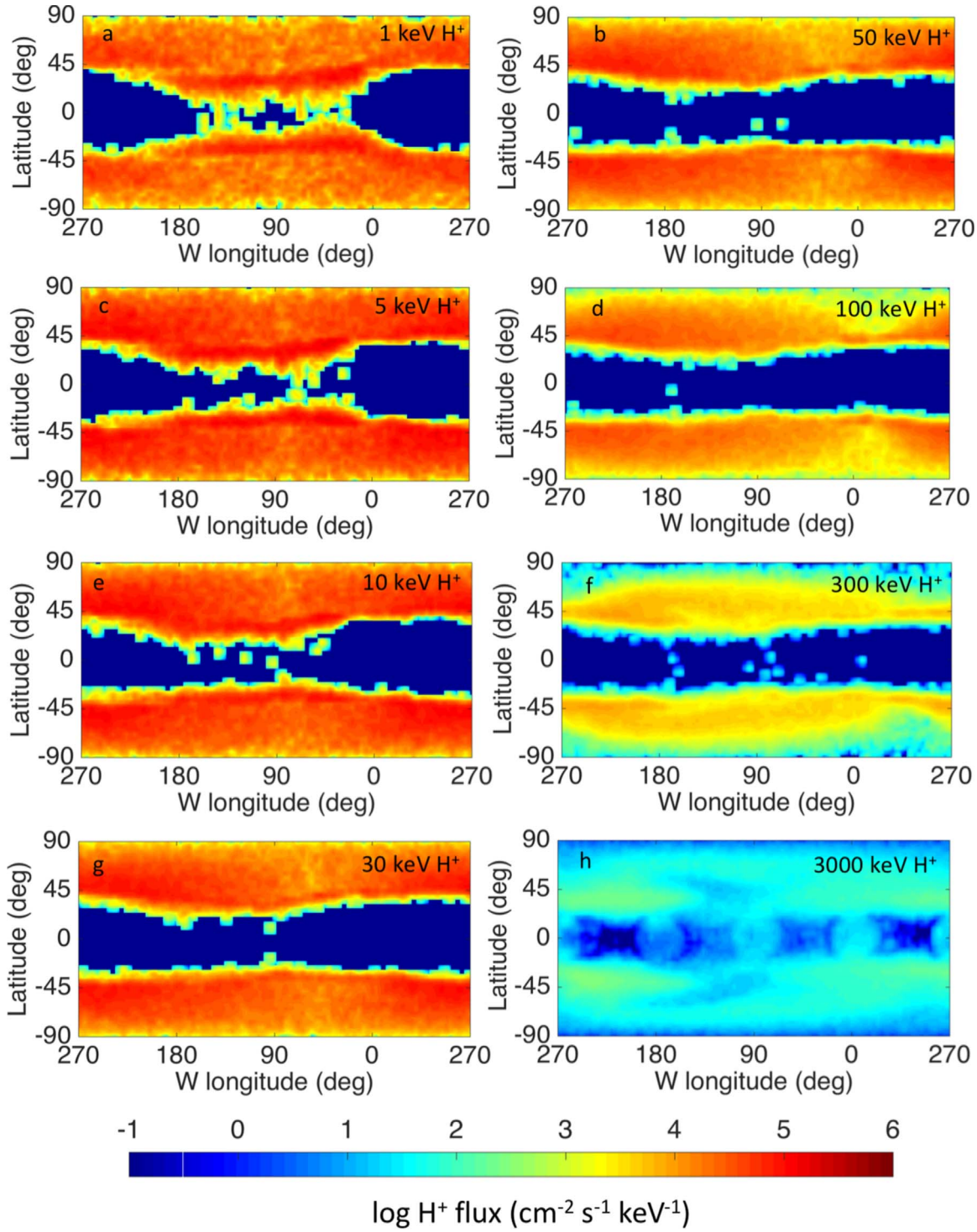

Figure 3. H^+ precipitation maps in science case (ii) (Ganymede is near the center of JPS) corresponding to different initial energies. Smaller granular structures in regions where the flux is very low (e.g., the equator) are caused by the finite number of test particles. The W longitude system has been used meaning the leading hemisphere is at long $\sim 90^0$ and long $\sim 0^0$ is at the Jupiter-facing hemisphere apex.

(plasma wake) hemisphere. Moreover, our results do not exclude the possibility that part of that redirected flow returns back also toward the trailing hemisphere.

Figure 5 presents the O^{++} precipitation to Ganymede's surface for the three considered configurations of the moon's magnetic field with respect to JPS, for initial ion energies 30 and 300 keV. The respective surface precipitation patterns are compatible with a flow guided strongly by the position of the OCFB. The surface precipitation of O^{++} at initial energy equal to 30 keV (Figure 5, panels (a), (c), and (e)) is in general asymmetric with respect to the leading and trailing hemispheres, as well as the Jupiter- and anti-Jupiter-facing sides of Ganymede's surface. As in the case of H^+, and even more markedly, for all the considered science cases, there is a significantly increased flow in the anti-Jupiter low-latitude and equatorial surface regions of the leading side of Ganymede

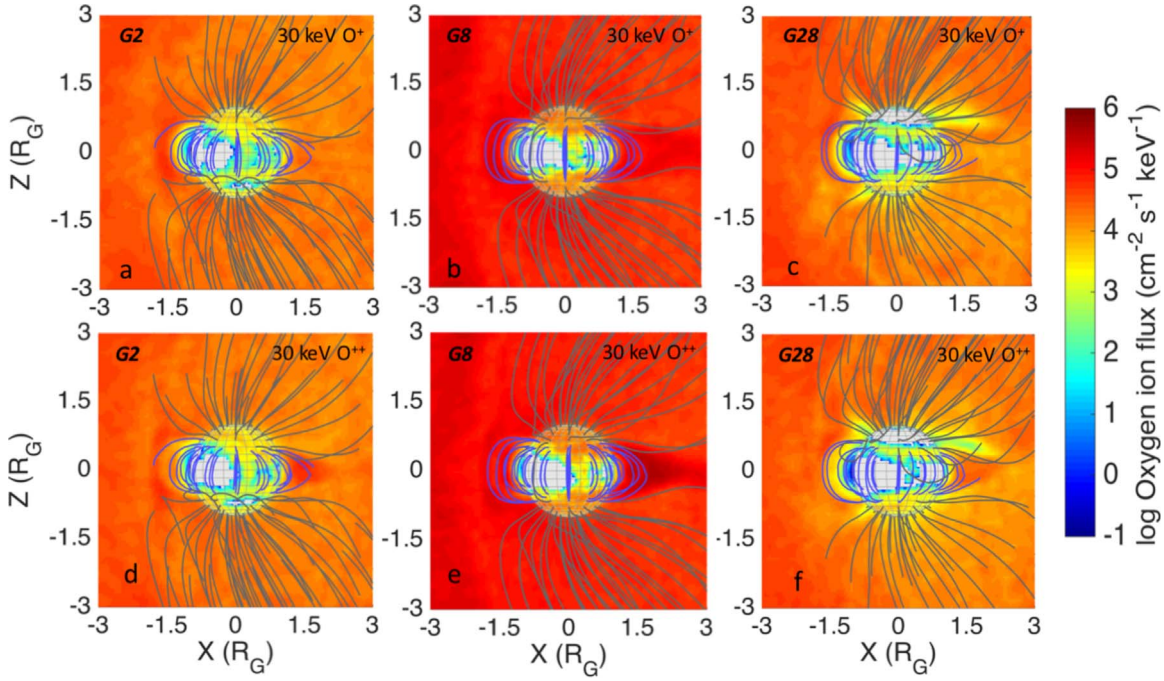

Figure 4. *XZ* projections of the O^+ and O^{++} circulation around Ganymede at initial energy equal to 30 keV for three different configurations of the moon's magnetic field with respect to JPS: panels (a) and (d) correspond to science case (i) (Ganymede is above the center of JPS); panels (b) and (e), correspond to science case (ii) (Ganymede is near the center of JPS); panels (c) and (f) correspond to science case (iii) (Ganymede is below the center of JPS). The GPhiO coordinates have been used: *X* is along the ambient flow direction (and Ganymede's orbital motion), *Z* is along Jupiter's spin axis, and *Y* points toward Jupiter (in units of Ganymede's radii).

(longitude range ∼ [90° 180°]; latitude range ∼[−45° 45°]). We note that this seems to apply also for science case (iii) (see Figure 5, panel (e)), although the statistics of the simulation do not allow a definite conclusion. In general, such an effect is expected for all types of ions and is due to the ion cyclotron motion and finite Larmor radius effects. Similar results are obtained also for the case of O^{++} at initial energy equal to 300 keV (Figure 5, panels (b), (d), and (f)); however, the aforementioned asymmetries are reduced, mainly due to the ions' higher magnetic rigidity. Indeed, the rigidity of the 300 keV O^{++} ions is ∼3.2 times the rigidity of the 30 keV O^{++} ions. For this reason, the 300 keV O^{++} ions get less affected by the magnetic field with respect to the lower-rigidity populations and consequently the maps of their precipitation to Ganymede's surface are less asymmetric. We note also that for science case (i), the heavy O^{++} flow at initial energy equal to 30 keV (see Figure 5, panel (a)) has local maxima within the trailing hemisphere, in its Jupiter-facing sector (270°W–360°W) for southern latitudes ∼65°S–45°S and in its anti-Jovian sector (180°W–270°W) for northern latitudes ∼40°N–55°N. An almost antisymmetric situation is noted for science case (iii) (see Figure 5, panel (e)): the flow has local maxima within the trailing hemisphere, in its Jupiter-facing sector (270°W–360°W) for northern latitudes ∼45°N–65°N and in its anti-Jovian sector (180°W–270°W) for southern latitudes ∼45°S–65°S.

In all three science cases, the surface precipitation of the O^{++} flux at initial energies equal to 30 and 300 keV takes place at higher latitudes at the trailing side with respect to the leading one. The flow downtail is strongly redirected near the equatorial plane. This result is consistent with simulations performed by Shay & Swisdak (2004), Paty et al. (2008), and Tóth et al. (2016). In general, the oxygen ion flux distribution on the low-latitude surface of the leading hemisphere, at both initial energies of 30 and 300 keV, is more extended than the one of hydrogen ions of the same energy (compare, for instance, Figure 5, panels (c) and (d) with Figure 3, panels (g) and (f)).

Figure 6 presents the S^{+++} precipitation to Ganymede's surface for the three considered configurations of the moon's magnetic field with respect to JPS, for initial ion energies equal to 30 keV (panels (a), (c), and (e)) and 300 keV (panels (b), (d), and (f)). As in the case of O^{++}, for all the considered science cases, there is a significantly increased flow in the anti-Jupiter low-latitude and equatorial surface regions of the leading hemisphere.

In conclusion, the majority of the H^+ impacts occur in the polar regions, due to their relatively low magnetic rigidity, which limits their capacity to penetrate in the closed field lines region. O^{++} and S^{+++}, due to their higher magnetic rigidity reach lower-latitude surface regions in the plasma downstream hemisphere; nevertheless, the main flux is still concentrated near the OCFB region. The asymmetries in the precipitating flux are attenuated as a function of both the particle rigidity and the configuration of Ganymede's magnetic field with respect to JPS.

4. Discussion

The results of the simulations performed in the context of the current study show a series of notable features in Ganymede's magnetosphere and reveal, for the first time, some important aspects of the variability of the ion–moon interactions, in terms of surface bombardment patterns. The results considering the case of Ganymede being near the center of JPS are qualitatively similar to those of other works where different methodological approaches have been followed (e.g., Fatemi et al. 2016; Poppe et al. 2018); nevertheless, some quantitative differences are existent. Below we discuss some of the main findings of the current work also through a comparison (where possible) with the results of past efforts.

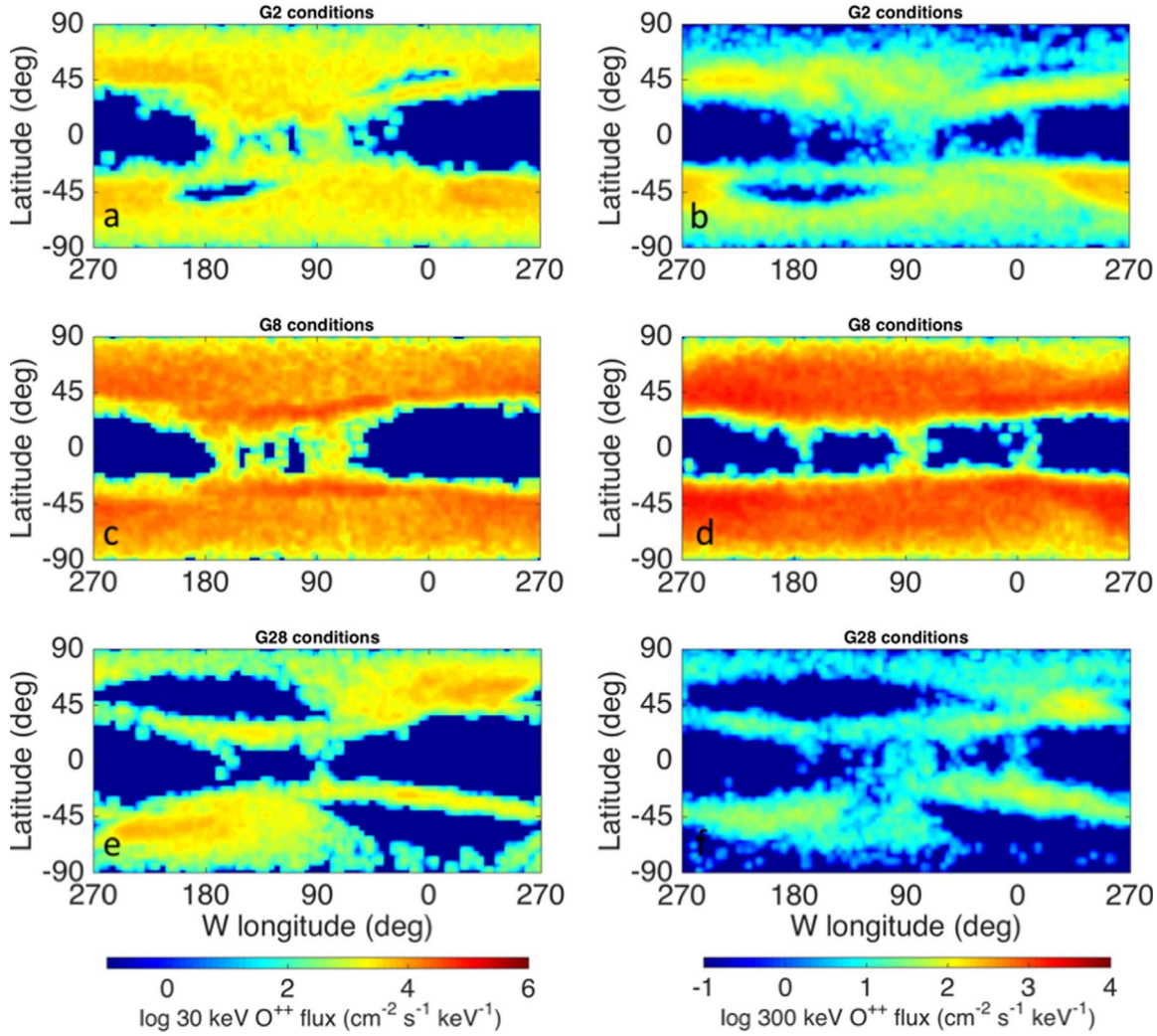

Figure 5. 30 keV O^{++} (panels (a), (c), and (e)) and 300 keV O^{++} (panels (b), (d), and (f)) precipitation to Ganymede's surface for different configurations of the moon's magnetic field with respect to JPS. Panels (a) and (b) correspond to magnetic field conditions similar to those during the Galileo G2 flyby (Ganymede above the center of JPS), panels (c) and (d) to those during the Galileo G8 flyby (Ganymede near the center of JPS), and panels (e) and (f) to those during the Galileo G28 flyby (Ganymede below the center of JPS). The W longitude system has been used, meaning the leading hemisphere is at long $\sim 90^0$ and long $\sim 0^0$ is at the Jupiter-facing hemisphere apex.

4.1. Confirmation of Previous Findings and Main Findings

The results of the current study, for all the considered configurations between Ganymede's magnetic field and JPS, confirm that the ion circulation above the moon's polar caps is strongly determined by the exact form of the Alfvén wings. Our particle trajectory simulations show that the Alfvén wings when Ganymede is above and below the center of JPS are not perfectly anti-asymmetric. This happens because the magnetic field in the Jupiter- and anti-Jupiter-facing sides is asymmetric (Jia et al. 2008).

Regions of lower or no ion flux inside the Alfvén wings are evident in the H^+ ion circulation maps in both science cases (i) and (iii) (see Figure 2, panels (c) and (i)) and also in the heavier ion circulation maps. Figure 7 shows the circulation maps of O^{++} at initial energy equal to 30 keV in science cases (i) and (iii). It is evident that cavities within the Alfvén wings depend both on the ion magnetic rigidity and the configuration of the moon's magnetic field with respect to JPS. Plasma cavities within the Alfvén wings have also been found in the simulations by Tóth et al. (2016) but not in the simulations by Fatemi et al. (2016). These two models (MHD and hybrid, respectively), show marked differences in the shape of the Alfvén wings and in the density distribution both within and outside the wings (readers can compare density and magnetic field line geometry plotted in Figure 1, panel (C), in Fatemi et al. 2016, with Figure 6 (upper panels) in Tóth et al. 2016). Our model, which is based on MHD-derived fields, in this context shows results that are more in accordance with Tóth et al. (2016).

The surface precipitation patterns for all three energetic ion species considered in this study show a large-scale dichotomy in surface fluxes between the polar and the lower-latitude regions of Ganymede. In particular, longitudinal variations in the width of the equatorial shielded region are observed between the precipitation maps of the three ion populations, with the widest latitudinal shielding occurring on the trailing hemisphere (plasma upstream) for ions with low initial rigidity (e.g., H^+) in science case (iii). The shielding of the equatorial region of the leading hemisphere depends not only on the initial ion rigidity but, possibly, also on the ion motion in the magnetotail toward the downstream surface.

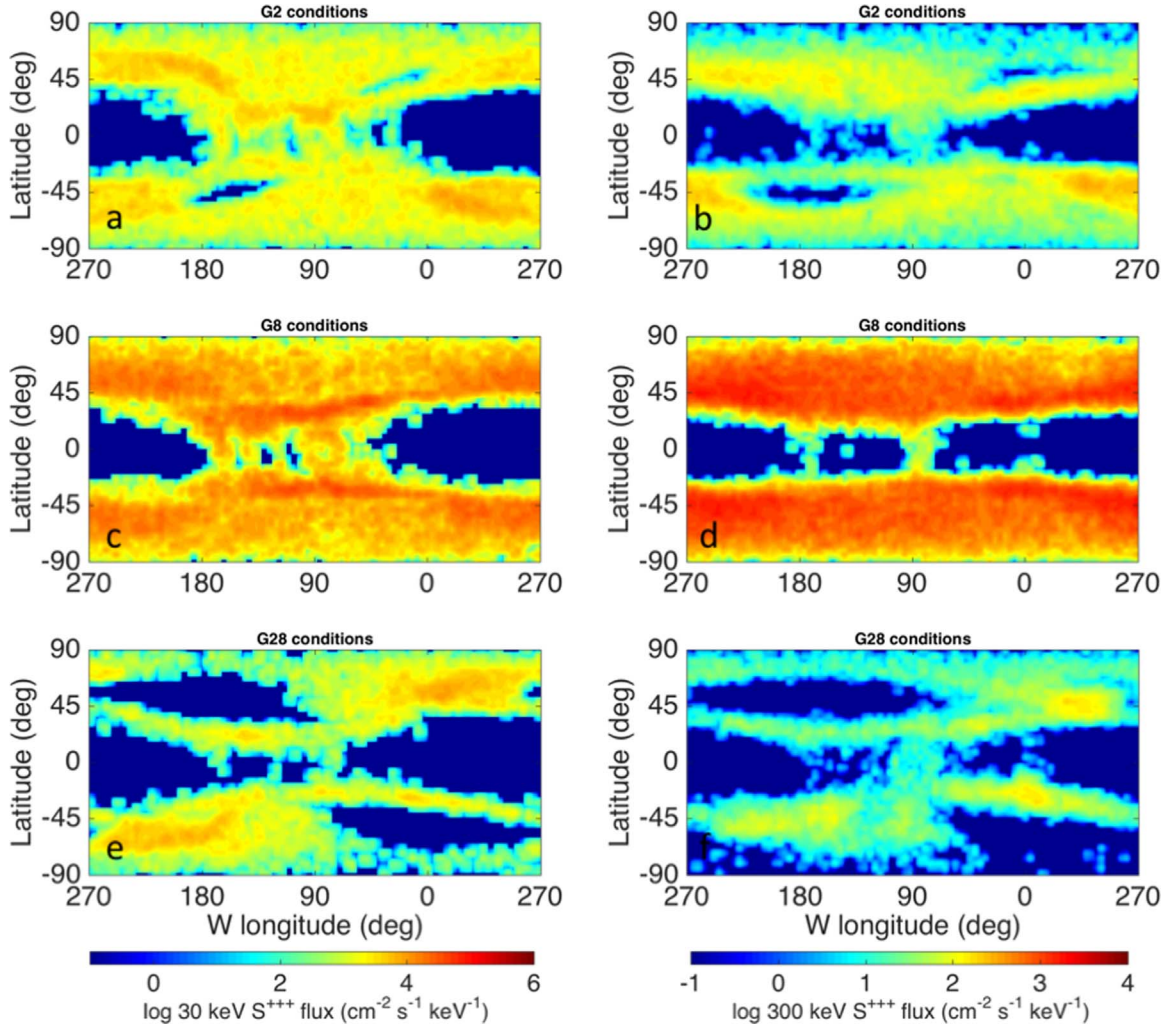

Figure 6. 30 keV S^{+++} (panels (a), (c), and (e)) and 300 keV S^{+++} (panels (b), (d), and (f)) precipitation to Ganymede's surface for different configurations of the moon's magnetic field with respect to JPS. Panels (a) and (b) correspond to magnetic field conditions similar to those during the Galileo G2 flyby (Ganymede above the center of JPS), panels (c) and (d) to those during the Galileo G8 flyby (Ganymede near the center of JPS), panels (e) and (f)) to those during the Galileo G28 flyby (Ganymede below the center of JPS). The W longitude system has been used meaning the leading hemisphere is at long $\sim 90^0$ and long $\sim 0^0$ is at the Jupiter-facing hemisphere apex.

In this work, we find that the magnetospheric ion fluxes are accelerated mainly toward the surface at the OCFB regions of both the trailing and leading hemispheres and in the magnetotail. The ion fluxes (in $cm^{-2}\,s^{-1}$), integrated in energy, precipitating to Ganymede's surface according to the simulation results of this work are presented in Table 1. The total ion precipitating rate on Ganymede's surface (in s^{-1}) for each science case and ion species is given in Table 2. We note that when Ganymede is near the center of JPS (science case (ii)), H^+ has the highest flux and the highest precipitation rate. The exact morphology of the ion precipitation patterns at the leading hemisphere depends on the configuration of Ganymede's magnetic field with respect to JPS. The simulations of the current work confirm qualitatively our past findings in Plainaki et al. (2015), which, however, referred only to science case (ii) and considered singly charged ions in a limited range of initial energies (1–100 keV). The current work, in addition, integrates our previous effort by considering three different configurations of the magnetic field plus a wide range of ion energies, including multiply charged heavy ions. Current simulations show that there is a longitudinal asymmetry between the ion precipitation in the low-latitude trailing and leading hemispheres, not only when Ganymede is near the center of JPS (see works by Fatemi et al. 2016; Poppe et al. 2018) but also when it is above or below it.

Figure 8 shows the low-energy H^+ precipitation maps in science case (i) (panels (a) and (c)) and science case (iii) (panels (b) and (d). In science cases (i) and (iii), hydrogen ions with initial energies 1 and 5 keV almost do not reach some midlatitude regions of the surface (see Figure 8, regions within the dashed circles). The existence of these "shielded areas" is due to the geometry of the electromagnetic fields, which, being tilted with respect to Ganymede's rotation axis, create specific access paths for the impinging populations. For each ion population of a specific magnetic rigidity, the form and position of these "shielded areas" are different, depending on the orientation of Ganymede's magnetic field with respect to JPS. Indeed, this effect is also evident in the heavy-ion populations (see, for instance, panels (a) and (e) of Figure 5 and panels (a) and (e) of Figure 6).

Our results considering science case (ii) are in agreement with the findings of other studies based either on hybrid simulations of Ganymede's magnetosphere (e.g., Fatemi et al. 2016) or single-particle models using either a self-consistent

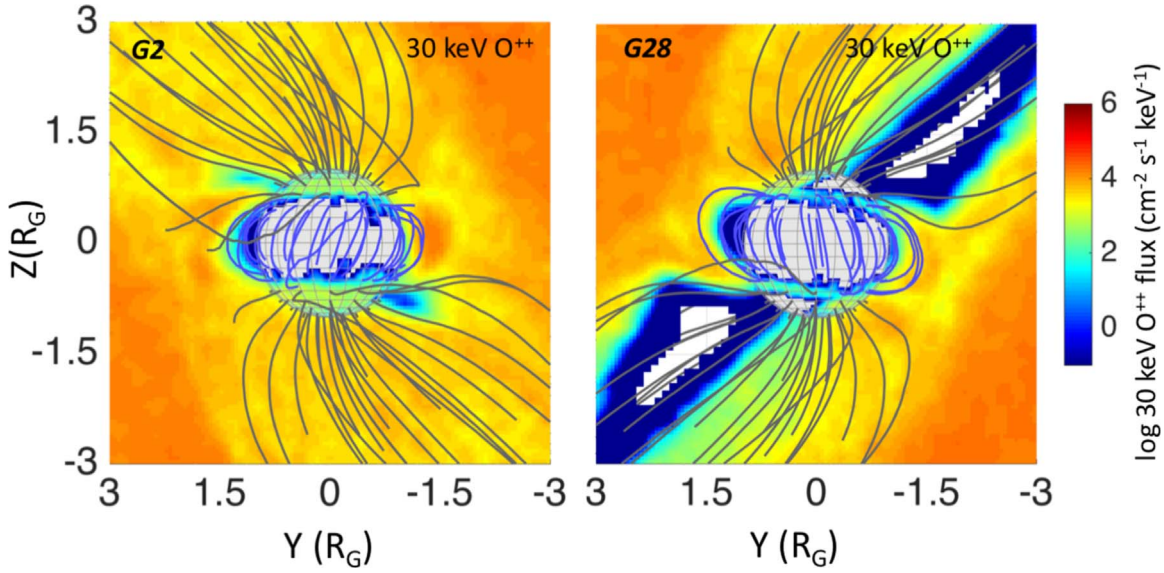

Figure 7. Circulation maps of O^{++} at initial energy equal to 30 keV in science case (i) (Ganymede above the center of JPS; left panel) and (iii) (Ganymede below the center of JPS; right panel). The GPhiO coordinates have been used: *X* is along the ambient flow direction (and Ganymede's orbital motion), *Z* is along Jupiter's spin axis, and *Y* points toward Jupiter (in units of Ganymede's radii).

plasma model (e.g., Poppe et al. 2018) or a superposition of Ganymede and Jovian magnetic fields as background fields (Allioux et al. 2013). In particular, the current study shows that in science case (ii), most of the O^{++} and S^{+++} low-latitude and equatorial flux precipitates on the anti-Jupiter-facing side of Ganymede's leading hemisphere, in agreement with results by Poppe et al. (2018). For the same science case (ii), we find that no low-energy ($E < 30$ keV) ion fluxes have access to Ganymede's low-latitude ($<20^0$) trailing hemisphere, in agreement with both Poppe et al. (2018) and Allioux et al. (2013), whereas they can impact the equatorial regions of the leading side. Protons with energies in the 30–300 keV range almost cannot reach Ganymede's surface in the equatorial regions of both the leading and trailing sides, in agreement with Poppe et al. (2018). We note that the results by Allioux et al. (2013) for 25, 300 keV, and 6 MeV $H^+$and O^{++} densities in the near-Ganymede space also display local depletions over the polar regions of Ganymede and near the "cusp" regions where the total fields reach a minimum in a simple superposition model of magnetic fields. Such a result may be due to the nonsimulation of ion bouncing between Ganymede's poles and Jupiter, similar to the nonmirroring case examined in Plainaki et al. (2015; see their Figure 2). In any case, the results of Allioux et al. (2013) show a general decrease in ion density as the ion energy increases, and this is qualitatively in agreement with the results of the current paper.

4.2. The Importance of Studying the Energetic H^+ Circulation

H^+ is the most abundant species in the near-Ganymede environment in the nonthermal energy range (i.e., above a few keV; see Poppe et al. 2018). Understanding the effects of energetic hydrogen ions on the interactions of Ganymede's surface and exosphere with the Jovian magnetosphere is of significant importance, also in the context of the study of planetary space weather within a giant planetary system (see, for instance, Plainaki et al. 2016 and references therein). In particular, the distribution of H^+ with an initial energy of 10 keV (see Figure 2) can be considered to be a good means of studying the influence of Ganymede's intrinsic magnetic field on the ion flux distribution in the near-surface environment. This is because the motion of these ions is driven by the magnetic field in a more significant way than the motion of heavier JPS ions, even when the latter are multiply charged (e.g., O^{++} or S^{+++}). This is due to the lower magnetic rigidity of H^+; in particular, the magnetic rigidity of H^+ is half of the rigidity of O^{++} under the same energy, and therefore, small-scale variations in the H^+ distributions should be in general more evident. We note that this applies for our single-particle MC model, whereas in the case of ideal MHD models, where ion cyclotron motion is averaged out and the ions and electrons are combined into a single fluid, such a difference between the circulation of light and heavy ions would not be present. Also, in the context of possible future planetary space weather measurements (e.g., with JUICE), with H^+ of low magnetic rigidity, the detection of its distribution in the near-Ganymede space would allow us to sense the short-term variability of the interactions between JPS and the moon itself. Indeed, such a measurement together with ENA imaging can provide a dynamic picture of Ganymede's magnetosphere, also as a function of the conditions external to the moon.

The total H^+ precipitation rate, in the energy range 1 keV–3 MeV, when Ganymede is near the center of JPS (science case (ii)), is estimated to be $3.6 \times 10^{24}\,s^{-1}$. The maximum H^+ flux is estimated to be $\sim 2.5 \times 10^7$ $cm^{-2}\,s^{-1}$. This value is somehow higher than the one estimated by Poppe et al. (2018) for the energetic H^+ population above the polar cap (8.4×10^6 $cm^{-2}\,s^{-1}$). This difference may be due to small differences in the energetic ion spectra used in the two works and/or to specific assumptions and modeling techniques. Indeed, because Poppe et al. (2018) assumed no ions being reflected back into the domain, their estimates may be considered as a lower bound and current results can serve as the upper bound. The energy spectrum by Paranicas et al. (1999) considered in the current work refers to H^+ energies higher than 1 keV, whereas the energy spectrum by Mauk et al. (2004) refers to H^+ energies higher than 10 keV. Of course, our "full mirroring" assumption probably leads to a relative

Table 1
Ion Fluxes, Integrated in Energy (in $cm^{-2}\,s^{-1}$), Precipitating to Ganymede's Surface According to the Simulation Results of this Work

Ion Species	Science Case (i) G2 Conditions		Science Case (ii) G8 Conditions		Science Case (iii) G28 Conditions	
	Flux (in $cm^{-2}\,s^{-1}$)		Flux (in $cm^{-2}\,s^{-1}$)		Flux (in $cm^{-2}\,s^{-1}$)	
	Average	Maximum	Average	Maximum	Average	Maximum
Hydrogen	2.9×10^5	3.9×10^6	4.3×10^6	2.5×10^7	4.1×10^4	3.9×10^5
Oxygen	1.8×10^5	1.1×10^6	1.4×10^6	5.7×10^6	8.0×10^4	5.9×10^5
Sulfur	2.6×10^5	1.4×10^6	1.5×10^6	5.7×10^6	1.4×10^5	8.3×10^5

Table 2
Total ion Precipitating Rate on Ganymede's Surface (in s^{-1})

Ion Species	Science Case (i) G2 Conditions	Science Case (ii) G8 Conditions	Science Case (iii) G28 Conditions
	Precipitation Rate (in s^{-1})	Precipitation Rate (in s^{-1})	Precipitation Rate (in s^{-1})
Hydrogen	2.5×10^{23}	3.6×10^{24}	3.2×10^{22}
Oxygen	1.6×10^{23}	1.2×10^{24}	6.9×10^{22}
Sulfur	2.3×10^{23}	1.4×10^{24}	1.2×10^{23}

overestimation of the flux precipitation on the polar surface; nevertheless, a nonmirroring assumption would lead to unrealistic situations as demonstrated in Plainaki et al. (2015).

The results of this study show that the H^+ flux with an initial energy of 10 keV is diverted by Ganymede's magnetic field at the distance of ~1.8–2 R_G from the moon's center in science cases (i) and (iii), whereas in science case (ii), the flux is reduced at a distance closer to the surface (i.e., at about 1.4 R_G from the surface; see Figure 2, panels (b), (e), and (h)). The width of the upstream magnetosphere in the simulations by Fatemi et al. (2016), who applied a three-dimensional self-consistent hybrid model of plasma where ions are treated as particles and electrons are considered as massless charge-neutralizing fluid, is somehow broader. Such difference may be attributed to the omission of energetic particles in the model of these authors, whereas the MHD models by Jia et al. (2008, 2009), from which the electromagnetic fields were extracted for our simulations, included the contribution of energetic particles to the total pressure in their model in order to obtain a simulated magnetosphere whose size is consistent with observations.

Our simulations also show enhanced hydrogen ion flows above the polar caps for all the considered science cases. Such a result confirms previous outcomes of hybrid simulations by Fatemi et al. (2016) corresponding to the G8 (Ganymede near the center of JPS) flyby of Galileo. In this paper, in addition, we present a new result: the ion precipitation on Ganymede's polar cap is more extended when Ganymede is above the center of JPS than when it is below. In reality, the entire precipitation patterns are different in these two cases, not only for H^+ but also for the heavy ions (see, for example, Figures 5 and 6). The total H^+ precipitation rate, however, is maximum in science case (ii) (see also Table 2).

4.3. Heavy Ions

Both energetic O^{++} and S^{+++} can penetrate Ganymede's magnetosphere down to the surface within the equatorial, closed field line region (i.e., at latitudes less than $\pm 30°$). Additionally, especially for science cases (i) and (ii), the flux of energetic O^{++} and S^{+++} into Ganymede's equatorial region shows local increases on the anti-Jupiter-facing leading hemisphere. This shift of the maximum equatorial precipitation away from the leading hemisphere apex toward the anti-Jupiter-facing hemisphere,is an indication of ions undergoing clockwise drift motion (as seen from the north) in addition to their bounce motion. In general, ions with larger rigidities have more probability of reaching the surface as they drift around Ganymede.

Our O^{++} and S^{+++} trajectory simulations corresponding to science case (ii) show the existence of pairs of narrow bands of ion precipitation at low latitudes ($\sim \pm 30°$) extending approximately from 0° to 180°W longitudes (that is the downstream hemisphere). This feature is particularly notable in populations of initial energy equal to 30 keV (see Figure 5, panel (c), and Figure 6, panel (c)). Such features have also been found in the results of other studies referring to similar conditions as the ones corresponding to our science case (ii) (e.g., Poppe et al. 2018). These features indicate the presence of ion populations that drift and bounce along Ganymede's closed field lines, as previously proposed by Poppe et al. (2018). These trapped charged particles comprise Ganymede's ionic radiation belts, in agreement also with the Galileo EPD observations of trapped-ion populations (Williams 2001, 2004). The equatorial bands in the precipitation maps in Figures 5, 6, and 8 actually show the footpoints of these belts on the surface, where ions with pitch angles within the loss-cone stop bouncing and hit the surface. The results of our model support the hypothesis put forward by Williams (2001) that Ganymede's ionic radiation belts are supplied by ions that are injected into Ganymede's magnetosphere through its magnetotail, where reconnection takes place (e.g., Jia et al. 2010b; Tóth et al. 2016). Indeed, modeling work has shown that the plasma convection in the tail is mainly governed by reconnection, which diverts part of the flow toward Ganymede and the rest downtail into the Jovian flow (Jia et al. 2010b). The flow that returns from the reconnection site toward Ganymede provides the source population of energized plasma, which may be streaming along the field lines and eventually precipitate onto the surface. So, the narrow precipitation bands evident in Figures 5 and 4 correspond to the magnetic footpoints of the open–closed field line boundaries, where particles with relatively small pitch angles can overcome the magnetic mirror force and precipitate to the surface of Ganymede.

5. Sputtering

The aforementioned results become of particular interest when speculating on the sputtering and surface-weathering

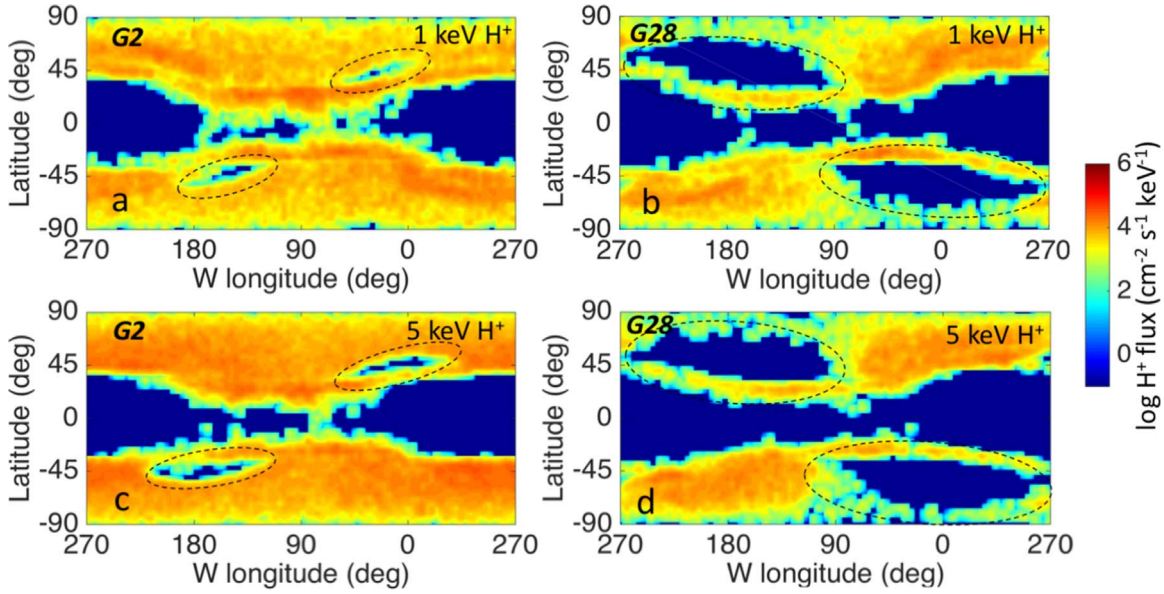

Figure 8. Low-energy H^+ precipitation maps in science case (i) (panels (a) and (c)) and science case (iii) (panels (b) and (d)). The regions indicated inside the dashed-line circles are regions with low or zero precipitating flux defined here as "shielded areas." For each ion population of a specific magnetic rigidity, the form and position of the "shielded areas" depend on the orientation of Ganymede's magnetic field with respect to JPS. The W longitude system has been used, meaning the leading hemisphere is at long $\sim 90^0$ and long $\sim 0^0$ is at the Jupiter-facing hemisphere apex.

processes at Ganymede. Energetic oxygen and sulfur ions can sputter the icy surface with high efficiency populating the moon's exosphere with H_2O molecules (Johnson 1990; Galli et al. 2016, 2017, 2018a, 2018b). The energetic particle radiation can also activate radiolytic processes in the upper surface layers, which are then followed by reactions among the water-dissociation products, resulting in the release of O_2, H_2, and other minor products (Cooper et al. 2001; Moore et al. 2007; Plainaki et al. 2015; Teolis et al. 2017; Galli et al. 2018a). Contrary to sputtering, radiolysis also depends strongly on the ice temperature. In this work, we investigate the effect of ion precipitation in releasing water molecules directly through sputtering, and we discuss our findings and their possible implications for weathering. The effect of Jovian energetic ions in releasing molecules through radiolysis, as well as the detailed generation and evolution of Ganymede's exosphere (see, for instance, Marconi 2007; Plainaki et al. 2015), goes beyond the scope of the current work and will be treated in a separate paper. Here we discuss some implications of the results of the current simulations, in terms of total precipitating flux patterns, on the surface's H_2O-sputtering capacity.

Figure 9 presents theoretical sputtered-H_2O yields corresponding to hydrogen, oxygen, and sulfur ions in a wide energy range, based on recent estimations by Teolis et al. (2017). The sputtering yield is defined here as the number of surface atoms or molecules released per impacting ion; it depends, among others, on the impacting ion's mass, energy, atomic number, and impacting angle, and the surface properties (Famá et al. 2008; Teolis et al. 2017). Taking into consideration our simulation results summarized in Table 2, we estimate the expected sputtering rates corresponding to different incident ions for different science cases. As shown in Table 3, the maximum sputtering rate all over the surface is expected during science case (ii).

To estimate the average sputtered-water rate, the individual rates corresponding to the three science cases, together with their relative weight during a complete period of the JPS

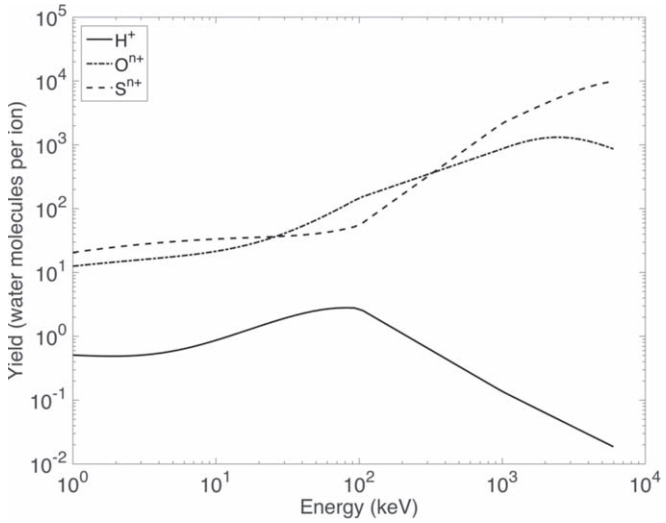

Figure 9. Water release yield due to the precipitation of H^+, O^{n+}, and S^{n+} in the energy range 1 keV–7 MeV. Yield values are from Teolis et al. (2017).

Table 3
Sputtered-water Rate on Ganymede's Surface (in s^{-1}) for Different Configurations of Ganymede's Magnetic Field with Respect to JPS

Ion Species	Science Case (i) G2 Conditions	Science Case (ii) G8 Conditions	Science Case (iii) G28 Conditions
	Sputtered-water Rate (in s^{-1})	Sputtered-water Rate (in s^{-1})	Sputtered-water Rate (in s^{-1})
Hydrogen	4.7×10^{23}	7.5×10^{24}	4.5×10^{22}
Oxygen	2.7×10^{25}	3.4×10^{26}	9.1×10^{24}
Sulfur	1.2×10^{25}	9.4×10^{25}	5.8×10^{24}
Total	3.9×10^{25}	4.4×10^{26}	1.5×10^{25}

movement upwards and downwards the moon's orbital plane, should be taken into account. We assume here that the average sputtering rate, A, may be given by the following expression:

$$A = \begin{cases} A_{G2} + (A_{G8} - A_{G2})|\cos(\omega t)|, & \omega t \in [0\ \pi) \\ A_{G28} + (A_{G8} - A_{G28})|\cos(\omega t)|, & \omega t \in [\pi\ 2\pi] \end{cases}, \quad (1)$$

where A_{G2} is the total sputtering rate during science case (i), A_{G8} is the total sputtering rate during science case (ii), and A_{G28} is the total sputtering rate during science case (iii) (see Table 3); and ω is the angular frequency of the JPS movement, equal to $\omega = 2\pi/T$, with T being Jupiter's rotation period, equal to ~9 hr 50 minutes, and t the time.

Averaging A over a complete period of the JPS movement, we find that the average sputtering rate of H_2O molecules from Ganymede's surface is $\sim 2.6 \times 10^{26}\,s^{-1}$.

This estimate is higher than our previous results in Plainaki et al. (2015), approximately by a factor of 3.7. This difference is due to the fact that we have considered an ionic population extending in a wider range of energies than the one previously considered. Heavier ions contribute more in sputtering than the lower-energy ones (see the behavior of the yield in Figure 9). We also note that in the estimates in Plainaki et al. (2015), which referred only to science case (ii), the considered impacting magnetospheric ion energy was limited to a maximum of 100 keV. Such an assumption resulted in a lower sputtering rate. Indeed, Figure 9 shows the importance in sputtering of ion energies higher than 100 keV, especially for the oxygen and sulfur ion species. Our current estimate is close to the sputtering rate value estimated by Poppe et al. (2018; $7 \times 10^{26}\,s^{-1}$); however, the results by Poppe et al. (2018) referred only to conditions similar to those during the Galileo G8 flyby. For this exact case, the sputtering rate estimates in this study are lower than those in Poppe et al. (2018) by a factor of ~1.6 (see Table 3, middle column). Such differences can be attributed to the different models used in each study and support, even if in an indirect way, the full mirroring assumption considered in both Plainaki et al. (2015) and the current paper which leads to results that are not extraordinarily different from those in other studies.

The average rate of the sputtered mass from Ganymede's surface is estimated to be equal to $7.8\,kg\,s^{-1}$. Assuming a direct escape fraction of 16.8% (Plainaki et al. 2015), we estimate a loss of the order of $1.3\,kg\,s^{-1}$. This value is significantly smaller than the one estimated for Europa, equal to $\sim 50\,kg\,s^{-1}$ (e.g., Schreier et al. 1993; Saur et al. 1998).

5.1. Ion Precipitation and Weathering

The current study confirms the existence of an equatorial asymmetry between the leading and trailing hemispheres in the ion precipitation maps, also during different configurations between Ganymede's magnetic field and JPS. This outcome is consistent with the past findings of a relatively bright leading hemisphere compared to a darker trailing one (Clark et al. 1986). However, due to the absence of new surface data, our knowledge on the detailed connection between the ion precipitation properties and spectroscopic weathering effects at Ganymede is limited at present.

Our results considering science case (ii) are also consistent with the surface albedo dichotomy observed by Voyager and Galileo between the bright polar caps and the relatively dark equatorial region (Smith et al. 1979; Johnson 1997; Khurana et al. 2007). Khurana et al. (2007) noted that the brightness boundary on Ganymede's surface corresponds closely to the OCFB line and argued that the sputtering and redistribution of water frost takes place onto optically thick material, hence resulting in a brightening of the moon's surface albedo. The results of the current paper do not contradict such a scenario, supported also by past simulations by Fatemi et al. (2016) and Poppe et al. (2018). Indeed, our simulations do show a precipitation guided by the magnetic field to the OCFB position; however, the border separating the highly accessible regions from the lower-latitude ones is not distinct. This happens because the precipitation depends strongly not only on the ion rigidity (depending on the ion species, energy, and charge state) but also on the configuration between Ganymede's magnetic field and JPS.

Ligier et al. (2019) studied the surface composition and properties of Ganymede performing linear spectral mixing modeling of a high-spectral-resolution data set, acquired with the near-infrared (1.40–2.50 μm) ground-based integral field spectrometer SINgle Faint Object Near-IR Investigation (SINFONI) of the Very Large Telescope (VLT hereafter) located in Chile. These authors found that the abundance maps of H_2O ice on Ganymede's surface are characterized by a latitudinal gradient linked to the impact of the external environment. In particular, they found that H_2O ice is nearly absent around the apex of the trailing hemisphere and tends to be less abundant near the equator (see Ligier et al. 2019, Figure 10(b)). Indeed, the abundance maps by Ligier et al. (2019) are well correlated with the heavy-ion precipitation patterns we estimate in this paper (see Figures 5 and 6). Moreover, our results confirm that the high-latitude surface regions and the leading side of Ganymede are more bombarded by heavy ions than the equatorial regions of the trailing side, also during different configurations between Ganymede's magnetic field and JPS (see Figures 5 and 6). The spatial distribution of the H_2O-sputtering rate is expected to follow the heavy-ion precipitation patterns, because the related yield increases with the ion mass (see Figure 8).

Below we further speculate on the role of the external environment in the H_2O-ice abundance distribution on Ganymede's surface. Ganymede displays a hemispherical albedo dichotomy with the trailing hemisphere being darker than the leading one (Calvin et al. 1995). Whereas Ganymede's surface has long been known to be dominated by H_2O ice (Kieffer & Smythe 1974; Pollack et al. 1978; Calvin et al. 1995), Galileo/NIMS observations have obtained evidence, for the first time, of the presence of CO_2 frost also (McCord et al. 1997, 1998; Hibbitts et al. 2003), which is preferentially hosted in non-icy low-albedo materials like hydrated salts and acids (McCord et al. 1998). Recent spectroscopic observations from the ground (Ligier et al. 2019) and from space, e.g., New Horizon/Lorri (Grundy et al. 2007) and Juno/JIRAM (Mura et al. 2020), have further confirmed the presence and geographical distribution of non-icy materials across the surface of Ganymede. Given the exponential dependence of water-ice sublimation on surface temperature, one would expect a more effective vapor production over the darker (and warmer) trailing hemisphere, unless segregation of water ice (Spencer 1987) occurs on these areas at spatial scales well below the resolution of the available spectroscopic data (essentially Galileo/NIMS and Voyager/IRIS). In particular, in the absence of substantial sputtering by energetic ions (e.g.,

in the low-latitude trailing-hemisphere regions), sublimated water will be transferred from the dark regions to the nearby brighter ones (e.g., Purves & Pilcher 1980; Shaya & Pilcher 1984), and this process will be terminated when the darker surface regions become largely covered in a lag deposit of non-ice particles that cut off further sublimation. Spencer (1987) showed that the result of this mechanism is the segregation of an initially fairly homogeneous surface into a patchwork of bright icy and dark ice-free areas over timescales from years to decades. The more contaminated areas therefore tend to become more and more depleted in ice, darker, and warmer, until an almost ice-free residual crustal layer is formed by compaction of the non-ice impurities previously dispersed in the ice matrix. While this dark layer can indeed reach rather high temperatures, its water release remains low. On the other hand, areas originally slightly brighter remain comparatively colder and therefore preferred for redeposition of water molecules from the exosphere, at least during the night. Moreover, these areas are subject to positive feedback, because newly deposited ice makes them increasingly brighter and colder. Given their lower temperatures, the bright areas experience a low water release rate. If these segregated areas are interspersed at scales below the spatial resolution of the currently available IR spectroscopic measurements, the net effect would be a reflectance spectra ($\lambda < 3$ μm) still displaying clear water-ice features (e.g., Ligier et al. 2019), while the thermal IR ($\lambda > 3$ μm) spectra would be dominated by the darker component, given the fourth-power dependence of thermal emission over temperature, therefore appearing warmer. Indeed, the decrease of Infrared Interferometer Spectrometer and Radiometer (IRIS) thermal IR spectra toward low wavenumbers (Spencer 1987) is a common feature of scenes characterized by strong subpixel temperature inhomogeneities. Such a scenario would be consistent with low water sublimation rates over the equatorial trailing hemisphere.

The competing ice redistribution process of ion sputtering can prevent segregation both in Ganymede's polar regions and in the equatorial leading hemisphere, which gets intensively bombarded by ions accelerated through magnetotail reconnection, as shown with our model (see Figures 5 and 6). Indeed, sputtering imposes more uniform redeposition conditions for water molecules during night (when sputtering arguably dominates over sublimation) and by extracting fresh ice from below the surface veneer. Overall, sputtering can maintain the uniformity of the overall albedo of the leading hemisphere surface, preventing the formation of ice-free compact layers and providing more favorable conditions for water release despite the lower temperatures of the surface. We conjecture that in the presence of water-ice segregation, such a sputtering-assisted sublimation mechanism as the one described above may be a plausible explanation to justify why the trailing-hemisphere low-latitude regions are more depleted in H_2O ice than the leading equatorial region. In addition, this scenario is in agreement with the observations by Ligier et al. (2019), who showed that the total H_2O-ice abundance map, composed of the sum of all grain sizes of both amorphous and crystalline H_2O ices, is well anticorrelated with the dark component's abundance distribution.

Of course, other exogenous processes may also play a role in the determination of the surface's brightness, such as ice excavation caused by micrometeoroid bombardment, as previously proposed by Ligier et al. (2019), preferentially occurring on the leading hemisphere (Bottke et al. 2013). Although there are currently not enough observations to constrain the feasibility of each proposed scenario, sputtering-assisted sublimation in the presence of water-ice segregation cannot be ruled out as a possible mechanism. Future measurements of the surface composition (e.g., with JUICE/MAJIS) and modeling work on the sputtering of carbonaceous material and formation, for example, of CO_2 ices will help explain the asymmetry in the brightness of the two hemispheres.

The results of the current study further confirm the asymmetric impact of radiation on the structure of surface water ice. The existence of amorphous ice—mostly in the first few-micrometer layers of Ganymede's surface regolith—may be due to higher radiation processing (Hansen & McCord 2004; Famá et al. 2010). Ligier et al. (2019) found that the amorphous ice distribution has a weakly higher abundance within the polar regions and a depletion in the equatorial trailing side (see their Figure 10(d)). Our results confirm that the polar regions (together with the leading equatorial side) are indeed more bombarded by energetic ions with respect to rest of the surface. Because the crystallization of water ice is expected to take place faster in the warmer equatorial regions, in the amorphous ice abundance maps in Ligier et al. (2019), large latitudinal differences could not be identified. Lastly, the strong latitudinal variation in the small (10–50 μm) grain size distribution by Ligier et al. (2019) is in agreement with our H^+ modeled precipitation maps with initial energies of 30–300 keV (see, for instance, Figure 3).

The modeled precipitation of heavy ions is also consistent with the study by Ligier et al. (2019). These authors inferred the possible and perhaps likely presence of sulfuric acid hydrate by matching the obtained spectra with a limited number of reference spectra. The enhanced abundance of this material just where the O^{++} and S^{+++} precipitation flux is more intense strongly supports its exogenic origin. A future detailed study of the surface molecule redistribution after sputtering and consequent effects on the surface optical properties may shed light on this argument. In this view, the current simulations may be used as a starting point for weathering studies when considering the magnetospheric ion precipitation pattern on the surface.

6. Summary and Concluding Remarks

In this paper, we apply a single-particle MC model (Plainaki et al. 2015) driven by the electromagnetic field from a well-established MHD model (Jia et al. 2008, 2009) to investigate the dynamics of the Jovian energetic ions in the near-Ganymede space and to estimate the precipitating flux on the moon's surface. For the first time, we perform energetic ion trajectory computations for three distinct configurations between Ganymede and JPS, characterized by magnetic and electric field conditions similar to those during the G2, G8, and G28 flybys of Galileo. The considered initial energies for the hydrogen, oxygen, and sulfur ions range from 1 keV to 3 MeV, and the spectra given by Paranicas et al. (1999) have been used.

The most important findings of the current work can be summarized as follows:

1. The surface precipitation patterns for H^+, O^{++}, and S^{+++} show a large-scale dichotomy in surface fluxes between the polar and the lower-latitude regions of Ganymede. Longitudinal variations in the width of the equatorial

shielded region are observed in the precipitation maps of the considered ion populations, with the widest latitudinal shielding occurring on the trailing hemisphere for ions with low initial rigidity (e.g., low-energy H^+) when Ganymede is below the center of JPS. The shielding of the equatorial region of the leading hemisphere (plasma downstream) depends not only on the initial rigidity of the ions but also on the magnetic field configuration with respect to JPS.

2. When Ganymede is above or below the center of JPS. the Alfvén wings are found to be not perfectly anti-asymmetric. This happens because the magnetic field in the Jupiter- and anti-Jupiter-facing sides is asymmetric (see also Jia et al. 2008). Regions of very low or zero flux inside the Alfvén wings when Ganymede is above or below the center of JPS, appear both in the H^+ (see Figure 2) and the heavier ion circulation maps (see, for instance, Figure 7).
3. The H^+ circulation and surface precipitation patterns are compatible with a flow guided by the magnetic field to the OCFB position. A relatively small contribution in the low-latitude surface precipitation on the leading side comes from the magnetotail direction. The H^+ precipitation on Ganymede's polar caps is more extended when Ganymede is above the center of JPS than when it is below. The low-energy H^+ precipitation on the high-latitude and polar cap surface regions presents a significant asymmetry between the Jupiter- and the anti-Jupiter-facing sides when Ganymede is above or below the center of JPS. Such an asymmetry is in the opposite sense for the case where the moon is above or below the center of JPS, and for the northern and southern hemispheres. This high-latitude and polar cap asymmetry is attenuated when Ganymede is near the center of JPS. In this case, the total precipitating flux is higher.
4. Features indicating the presence of trapped-ion populations in Ganymede's closed field line region, as previously proposed by Poppe et al. (2018) and in agreement also with the Galileo EPD observations (Williams 2001), have been found in the heavy-ion circulation maps corresponding to science case (ii). The equatorial bands in the precipitation maps in Figures 5 and 6 actually show the footpoints of these belts on the surface, extending at low latitudes ($\sim\pm30^\circ$) of the downstream hemisphere and being particularly notable in the populations of initial energy equal to 30 keV (see Figure 5, panel (c), and Figure 6, panel (c)). They correspond to the magnetic footpoints of the open–closed field line boundaries.
5. The surface precipitation of oxygen ions depends strongly on their actual charge state. The O^{++} precipitation patterns are also compatible with a flow through the polar caps and from the magnetotail, mainly through tail reconnection. The exact morphology depends strongly on the configuration of Ganymede's magnetic field with respect to JPS. The O^{++} flow gains access mainly through the OCFB region; in the magnetotail, ions are redirected along the closed field lines back to Ganymede's surface (see Figures 5 and 6), mainly through tail reconnection (e.g., Jia et al. 2010b; Tóth et al. 2016). A similar situation is also observed in the simulation results considering the S^{+++} case (see Figure 7). This phenomenon may be of interest from a comparative planetary space weather perspective.
6. Current simulations show that the overall precipitation is more intense when Ganymede is near the center of JPS. The low-latitude and equatorial surface precipitation flux always appears more intense in the anti-Jupiter direction, at least for initial ion energies lower than 300 keV. This shift of the maximum equatorial precipitation away from the leading hemisphere apex toward the anti-Jupiter-facing hemisphere may be an indication of ions undergoing clockwise drift motion (as seen from the north) in addition to their bounce motion. In general, ions with larger rigidities have more probability of reaching the surface as they drift around Ganymede. We conclude, therefore, that the access of JPS ions to Ganymede's surface is permanently antisymmetric between the Jupiter- and anti-Jupiter-facing hemispheres, with detailed characteristics that depend strongly on the moon's position with respect to JPS and the ion rigidities.
7. The average sputtering rate of H_2O molecules from Ganymede's surface over a complete period of the JPS movement up and down the moon is $\sim 2.6 \times 10^{26}\ s^{-1}$. The spatial distribution of the H_2O-sputtering rate is expected to follow well the heavy-ion precipitation patterns, as the related yield increases with the ion mass. The heavy-ion precipitation patterns estimated in this paper are well correlated with water abundance maps produced on the basis of SINFONI/VLT/ESO observations (Ligier et al. 2019), indicating that H_2O ice is nearly absent around the apex of the trailing hemisphere and tends to be less abundant near the equator.

The results of the current work may help us better understand the nature of ion–moon interactions in Jupiter's magnetosphere, their dynamic behavior, and the related implications from a planetary space weather perspective. However, further theoretical work focusing on the study of reconnection and particle acceleration inside Ganymede's magnetosphere is necessary to shed light on the processes characterizing ion–moon interactions. Recent efforts (e.g., Kaweeyanun et al. 2020) showed that the average reconnection rate is a function of Ganymede's position along its orbit around Jupiter, being driven by Jupiter's rotation. Future joint analysis of such effects on the ion precipitation on Ganymede's surface would be very important in order to have more accurate predictions of the related surface signatures, in preparation for the JUICE mission of ESA (Grasset et al. 2013).

Particle precipitation may be considered to be the key parameter determining the sputtering of water molecules, an important exosphere source for the Galilean satellites (e.g., Shematovich et al. 2005; Plainaki et al. 2012; Shematovich 2016 and references therein). Its variability also has direct impact on exosphere generation and evolution. Knowledge of the joint system of Jupiter's magnetosphere and Ganymede's environment (magnetosphere–exosphere surface) is of significant importance during the design of future missions to this Galilean moon and the planning of observations (see, for example, the discussion in Plainaki et al. 2016). Knowledge of the planetary space weather in the context of outer solar system exploration is also necessary for related environment specification studies and definition of possible countermeasures.

We thank the editor and referee for useful comments that improved the quality of the paper. Part of the research work in this paper has been carried out in the context of the ASI-INAF n.2018-25-HH.0 contract.

ORCID iDs

Christina Plainaki https://orcid.org/0000-0003-1483-5052
Stefano Massetti https://orcid.org/0000-0002-7767-1334
Xianzhe Jia https://orcid.org/0000-0002-8685-1484
Alessandro Mura https://orcid.org/0000-0002-4552-4292
Anna Milillo https://orcid.org/0000-0002-0266-2556
Davide Grassi https://orcid.org/0000-0003-1653-3066
Giuseppe Sindoni https://orcid.org/0000-0002-3348-7930
Emiliano D'Aversa https://orcid.org/0000-0002-5842-5867
Gianrico Filacchione https://orcid.org/0000-0001-9567-0055

References

Allioux, R., Louarn, P., & André, N. 2013, AdSpR, 51, 1204
André, N., Grande, M., Achilleos, N., et al. 2018, P&SS, 150, 50
Bagenal, F., Wilson, R. J., Siler, S., et al. 2016, JGRE, 121, 871
Boris, J. P. 1970, MATT-769 Technical Report (4168374), NSA-24-023976 (N.J. Plasma Physics Lab.: Princeton Univ.)
Bottke, W. F., Vokrouhlický, D., Nesvorný, D., & Moore, J. M. 2013, Icar, 223, 775
Calvin, W. M., Clark, R. N., Brown, R. H., et al. 1995, JGR, 100, 19041
Carnielli, G., Galand, M., Leblanc, F., et al. 2019, Icar, 330, 42
Carnielli, G., Galand, M., Leblanc, F., et al. 2020, Icar, 343, 113691
Chen, J., & Palmadesso, P. J. 1986, JGR, 91, 1499
Clark, R. N., Fanale, F. P., & Gaffey, M. J. 1986, in IAU Coll. 77, Some Background about Satellites, ed. J. A. Burns & M. S. Matthews (Tucson, AZ: Univ. Arizona Press), 437
Collier, M. R., & Hamilton, D. C. 1995, GeoRL, 22, 303
Collinson, G., Paterson, W. R., Bard, C., et al. 2018, GeoRL, 45, 3382
Cooper, J. F., Johnson, R. E., Mauk, B. H., et al. 2001, Icar, 149, 133
Dorelli, J. C., Glocer, A., Collinson, G., et al. 2015, JGRA, 120, 5377
Eviatar, A., Vasyliūnas, V. M., & Gurnett, D. A. 2001, P&SS, 49, 327
Famá, M., Loeffler, M. J., Raut, U., et al. 2010, Icar, 207, 314
Famá, M., Shi, J., & Baragiola, R. A. 2008, SurSc, 602, 156
Fatemi, S., Poppe, A. R., Khurana, K. K., et al. 2016, GeoRL, 43, 4745
Frank, L. A., Paterson, W. R., Ackerson, K. L., et al. 1997, GeoRL, 24, 2151
Galli, A., Vorburger, A., Pommerol, A., et al. 2016, P&SS, 126, 63
Galli, A., Vorburger, A., Wurz, P., et al. 2017, Icar, 291, 36
Galli, A., Vorburger, A., Wurz, P., et al. 2018a, Icar, 312, 1
Galli, A., Vorburger, A., Wurz, P., et al. 2018b, P&SS, 155, 91
Gomis, O., Satorre, M. A., Strazzulla, G., et al. 2004, P&SS, 52, 371
Grasset, O., Dougherty, M. K., Coustenis, A., et al. 2013, P&SS, 78, 1
Grundy, W., Buratti, B., Cheng, A., et al. 2007, Sci, 318, 234
Gurnett, D. A., Kurth, W. S., Roux, A., et al. 1996, Natur, 384, 535
Hall, D. T., Feldman, P. D., McGrath, M. A., et al. 1998, ApJ, 499, 475
Hansen, G. B., & McCord, T. B. 2004, JGR, 109, E01012
Hibbitts, C. A., Pappalardo, R. T., Hansen, G. B., et al. 2003, JGR, 108, 5036
Jia, X., Kivelson, M. G., Khurana, K. K., et al. 2010a, SSRv, 152, 271
Jia, X., Walker, R. J., Kivelson, M. G., et al. 2008, JGR, 113, A06212
Jia, X., Walker, R. J., Kivelson, M. G., et al. 2009, JGR, 114, A09209
Jia, X., Walker, R. J., Kivelson, M. G., et al. 2010b, JGRA, 115, A12202
Johnson, R. E. 1990, Energetic Charged-Particle Interactions with Atmospheres and Surfaces (Berlin: Springer)
Johnson, R. E. 1997, Icar, 128, 469
Kaweeyanun, N., Masters, A., & Jia, X. 2020, GeoRL, 47, e2019GL086228
Keppler, E., & Krupp, N. 1996, P&SS, 44, 71
Khurana, K. K., Pappalardo, R. T., et al. 2007, Icar, 191, 193
Kieffer, H. H., & Smythe, W. D. 1974, Icar, 21, 506
Kivelson, M. G., Bagenal, F., Kurth, W. S., et al. 2004, in Jupiter: The planet, satellites, and Magnetosphere, ed. R. E. Johnson et al. (Cambridge: Cambridge Univ. Press), 513
Kivelson, M. G., Khurana, K. K., Coroniti, F. V., et al. 1997, GeoRL, 24, 2155
Kivelson, M. G., Khurana, K. K., Russell, C. T., et al. 1996, Natur, 384, 537
Kivelson, M. G., Warnecke, J., Bennett, L., et al. 1998, JGR, 103, 963
Kliore, A. J. 1998, HiA, 11, 1065
Leblanc, F., Oza, A. V., Leclercq, L., et al. 2017, Icar, 293, 185
Ligier, N., Paranicas, C., Carter, J., et al. 2019, Icar, 333, 496
Marconi, M. L. 2007, Icar, 190, 155
Mauk, B. H., Mitchell, D. G., McEntire, R. W., et al. 2004, JGR, 109, A09S12
McCord, T. B., Carlson, R. W., Smythe, W. D., et al. 1997, Sci, 278, 271
McCord, T. B., Hansen, G. B., Clark, R. N., et al. 1998, JGR, 103, 8603
McGrath, M. A., Xianzhe, J., Retherford, K., et al. 2013, JGRA, 118, 2043
Moore, M. H., Hudson, R. L., & Carlson, R. W. 2007, Icar, 189, 409
Mura, A., Adriani, A., Sordini, R., et al. 2020, JGR, submitted
Paranicas, C., Paterson, W. R., Cheng, A. F., et al. 1999, JGR, 104, 17459
Paty, C., Paterson, W., & Winglee, R. 2008, JGR, 113, A06211
Paty, C., & Winglee, R. 2004, GeoRL, 31, L24806
Plainaki, C., Cassidy, T. A., Shematovich, V. I., et al. 2018, SSRv, 214, 40
Plainaki, C., Lilensten, J., Radioti, A., et al. 2016, JSWSC, 6, A31
Plainaki, C., Milillo, A., Massetti, S., et al. 2015, Icar, 245, 306
Plainaki, C., Milillo, A., Mura, A., et al. 2012, Icar, 218, 956
Plainaki, C., Sindoni, G., Grassi, D., et al. 2020, P&SS, 191, 105004
Pollack, J. B., Witteborn, F. C., Erickson, E. F., et al. 1978, Icar, 36, 271
Poppe, A. R., Fatemi, S., & Khurana, K. K. 2018, JGRA, 123, 4614
Purves, N. G., & Pilcher, C. B. 1980, Icar, 43, 51
Saur, J., Strobel, D. F., & Neubauer, F. M. 1998, JGR, 103, 19947
Schreier, R., Eviatar, A., Vasyliunas, V. M., & Richardson, J. D. 1993, JGR, 98, 21231
Shay, M. A., & Swisdak, M. 2004, PhRvL, 93, 1
Shaya, E. J., & Pilcher, C. B. 1984, Icar, 58, 74
Shematovich, V. I. 2016, SoSyR, 50, 262
Shematovich, V. I., Johnson, R. E., Cooper, J. F., & Wong, M. C. 2005, Icar, 173, 480
Shi, M., Baragiola, R. A., Grosjean, D. E., et al. 1995, JGR, 100, 26387
Smith, B. A., Soderblom, L. A., Beebe, R., et al. 1979, Sci, 206, 927
Spencer, J. R. 1987, Icar, 69, 297
Teolis, B. D., Plainaki, C., Cassidy, T. A., et al. 2017, JGRE, 122, 1996
Tóth, G., Jia, X., Markidis, S., et al. 2016, JGRA, 121, 1273
Turc, L., Leclercq, L., Leblanc, F., et al. 2014, Icar, 229, 157
Williams, D. J. 2001, GeoRL, 28, 3793
Williams, D. J. 2004, JGRA, 109, 9211
Williams, D. J., Mauk, B. H., McEntire, R. W., et al. 1997, GeoRL, 24, 2163
Williams, D. J., McEntire, R. W., Jaskulek, S., et al. 1992, SSRv, 60, 385
Zhou, H., Tóth, G., Jia, X., Chen, Y., & Markidis, S. 2019, JGRA, 124, 5441